Oxygen transfer in ferric iron biological production in a packed-bed reactor

A.Mazuelos, R. Romero, I. Palencia, F. Carranza, F.J. Borjas

Dpto. De Ingeniería Química. Facultad de Química. Universidad de Sevilla. Sevilla 41012. Spain.

Abstract

In this paper oxygen transfer in the ferrous iron biooxidation process in a packed bed reactor is studied. The reactor consists of a polymethyl methacrylate column randomly packed with siliceous stone particles with inlets for liquid medium and air at the bottom from where they flood the reactor.

The aim of this work is to determine the parameters that influence the oxygen transfer from air bubbles to the liquid medium, and to characterize the oxygen transport through the bulk liquid medium.

Keywords: biooxidation, oxygen transfer, packed-bed, bioreactor

1. Introduction

Ferric iron can be used as oxidising agent in hydrometallurgical leaching operations (Carranza et al., 1993; Iglesias et al., 1996) ($MS + 2Fe^{3+} \rightarrow M^{2+} + S^0 + 2Fe^{2+}$) and in the removal of hydrogen-sulphide in combustible gases (Magota and Shiratori, 1988) ($2Fe^{3+} + SH_2 \rightarrow 2Fe^{2+} + S^0 + 2H^+$). In these processes, the ferric iron consumed can be regenerated by the biological oxidation (by *Thiobacillus ferrooxidans* and other ferrooxidant bacteria) of the ferrous iron produced ($2Fe^{2+} + ½\ O_2 + 2H^+ \rightarrow$

$2Fe^{3+} + H_2O$). In this way, both processes are closed treatments (Fig. 1). The economic viability of these processes depends strongly on the biooxidation efficiency.

The highest ferric iron productivity found in the literature (Livesey-Goldblatt et al., 1979; Lancy and Tuovinen 1984; Nakamura et al., 1986; Nikolov et al., 1988; Grishin and Tuovinen, 1988; García et al., 1989; Carranza and García, 1990; Karamanev, 1991; Armentia and Webb, 1992; Gómez and Cantero, 1999; Mazuelos et al., 1999, 2000, 2001) was obtained in a bioreactor that consisted of a column packed with siliceous stone particles with inlets for liquid medium (ferrous iron solution) and air at the bottom (Mazuelos, 2000). In this bioreactor, the liquid and air flow rates were simultaneously increased stepwise. Air flow rate had a noticeable effect on ferric iron productivity, which increased as the air flow rate increased. The authors concluded that the biooxidation process was limited by the availability of oxygen in the liquid medium.

Oxygen transfer is the key to aerobic biological processes, especially at high cell densities when cell growth is likely to be limited by availability of oxygen in medium; therefore the understanding of the phenomena implied in the oxygen transfer is essential for the design of these reactors.

The present work studies the parameters that influence the oxygen transfer from air bubbles to the liquid medium and the characterization of the oxygen transport through the bulk liquid medium in a packed-bed reactor, in which the geometrical design details, operating conditions and liquid medium composition were similar, as far as possible, to those of the bioreactor studied by Mazuelos et al. (2000) for the ferrous iron biooxidation.

2. Materials

2.1. Reactor

The reactor was similar to that used by Mazuelos et al. (2000) except for the biofilm formed on the solid support.

The reactor consisted of a 1249 mm high and 84 mm diameter polymethyl methacrylate column randomly packed with siliceous stone particles of 6-7 mm in size. The reactor was divided into four zones, named zero, first, second and third floor. First, second and third floors were packed-beds each 280 mm high, in which the porosity was 0.42. A 45 mm high empty space separated each bed floor from the next one. The packing of each floor was supported by plastic screens. The air diffuser was placed at the bottom of the column, inside the zero floor. Zero floor was a space without support particles. The air diffuser was a wood prism (4.3 x 1.5 x 1.5 cm) from whose pores emerged the air bubbles. Air was supplied under pressure (0.5 bar) by a compressor. The liquid medium was fed at the bottom of the column by a peristaltic pump and went out by a hole (by overflow) placed above the third floor. The reactor was placed in a thermostatically controlled room, the temperature of which was maintained at 31ºC.

2.2. Liquid medium

The liquid medium was a ferrous sulphate acid solution with 8 g/L of ferrous iron and pH 1.25 adjusted with sulphuric acid.

3. Methods

3.1. Bubble size distribution

The air bubble size distribution was experimentally studied for packed-bed heights (h) of 0 to 84 cm.

The experimental procedure was as follows: a packed-bed h cm high was made with support particles. Then, liquid medium was added to fill the column and the air flow rate was set at 1.1 L/min. Bubble images were obtained by filming the zone on top of the packed-bed by a video camera (Oliveira and Ni, 2001) with the aim of measuring the air bubbles that left the packed-bed. To obtain a representative bubble size distribution (BSD), the diameter of 200 bubbles randomly selected was measured using a TV-monitor.

3.2. Volume occupied by gas

The volume of gas inside the reactor (V_G) was determined at packed-bed heights ($h´$) of 0 to 84 cm. The experimental procedure was as follows: the column was filled with liquid medium and a packed-bed $h´$ cm high was made with support particles. The liquid level was adjusted up to 0.5 cm above the packed-bed. Air was supplied at a flow rate of 1.1 L/min. The volume occupied by air was determined by measuring the changes in the liquid height with a fine scale fixed on the column (Oliveira and Ni, 2001). The procedure involves measuring the liquid level without the presence of gas and the corresponding level when gas is continuously introduced at a given flow rate.

3.3. Gas-liquid interfacial area

In a bubble size distribution, each bubble size, characterized by the bubble diameter d_i, is associated to a frequency of appearance, f_i, or bubble number fraction, defined as

$$f_i = n_i / 200 \quad (1)$$

where n_i is the number of bubbles with size d_i. The mean bubble diameter, d_b, is calculated according to

$$d_b = \Sigma(d_i \cdot f_i) \quad (2)$$

The total interfacial area for oxygen transfer is the gas-liquid interfacial area which is a function of the total volume of gas in the system as well as of the bubble size distribution. The gas-liquid interfacial area in a given section of the column between heights j and k, A_{jk}, is given by

$$A_{jk} = a_{jk} \cdot (V_G)_{jk} \quad (3)$$

where a_{jk} and $(V_G)_{jk}$ are the mean specific interfacial area and the volume of gas bubbles respectively in the section [j-k] of the column. They are calculated from

$$a_{jk} = (a_j + a_k)/2 \quad (4)$$

$$(V_G)_{jk} = (V_G)_k - (V_G)_j \quad (5)$$

where a_j and a_k are the specific interfacial area for heights *j* and *k*, calculated from equation (6), and $(V_G)_k$ and $(V_G)_j$ are the total volume of gas bubbles at heights *j* and *k* measured experimentally.

The specific interfacial area at a height *h* is calculated according to

$$a_h = \frac{S_h}{V_h} = \frac{\pi \cdot n_{Th} \cdot \sum d_{ih}^{\,2} \cdot f_{ih}}{1/6 \cdot \pi \cdot n_{Th} \cdot \sum d_{ih}^{\,3} \cdot f_{ih}} = 6 \cdot \frac{\sum d_{ih}^{\,2} \cdot f_{ih}}{\sum d_{ih}^{\,3} \cdot f_{ih}} \qquad (6)$$

where S_h is the average surface area of bubbles at height *h*, V_h is the average volume of bubbles at height *h*, and n_{Th} is the total number of bubbles at height *h*.

3.4. Effect of the column height on the mass transfer coefficient value

The general expression for the gas-liquid transfer rate of a component A can be simplified for systems in which most of the resistance lies in the liquid phase film: if A is poorly soluble in the liquid, e.g. oxygen in aqueous solution, the liquid phase mass-transfer resistance dominates and the gas-liquid oxygen transfer rate, ν, can be calculated from the following equation:

$$\nu = k_L \cdot A \cdot (c_L^{\,*} - c_L) \qquad (7)$$

where k_L is the liquid-phase mass-transfer coefficient, A is the gas-liquid interfacial area, c_L is the oxygen concentration in the liquid medium and $c_L^{\,*}$ is the oxygen concentration in the liquid medium in equilibrium with the gas phase, that is, the oxygen solubility in the liquid medium.

The rate of oxygen transfer is influenced by several physical and chemical factors that change either the value of k_L or the value of A, or the driving force for mass transfer, $(c_L^* - c_L)$. For a given set of operating conditions, the maximum rate of oxygen transfer occurs when the concentration difference driving force $(c_L^* - c_L)$ is highest, i.e. when the concentration of dissolved oxygen, c_L, is zero.

Titanium (III) is a powerful reducing agent and reacts instantaneously with the oxygen dissolved in the liquid medium according to the equation:

$$4\ Ti^{3+} + O_2 + 6\ H_2O \rightarrow 4\ TiO_2 + 12\ H^+$$

therefore, an excess of Ti^{3+} assures a null concentration of oxygen in the liquid medium. A set of assays were carried out for several packed-bed heights, in which the liquid medium was mixed with a 15% w/w $TiCl_3$ in concentrated hydrochloric acid solution in a volumetric ratio of 93.3/6.7 (liquid medium/$TiCl_3$ solution). Air and liquid flow rates were 1.1 L/min and 2.4 L/h respectively and the reactor operated in continuous mode. In the experiment, the titanium concentration in liquid flowing to and from the reactor was measured. For a packed-bed height j, from a mass balance at steady state, the difference in titanium flow between inlet and outlet must be equal to the titanium oxidation rate and to the maximum oxygen transfer rate from gas to liquid:

$$v_j = F_l \cdot ([Ti^{3+}]_i - [Ti^{3+}]_o) = k_L \cdot A \cdot c_L^* \qquad (8)$$

where F_l is the volumetric liquid flow rate, $[Ti^{3+}]$ is the concentration of titanium in the liquid medium, and subscripts i and o refer to inlet and outlet liquid streams respectively.

Gas-liquid oxygen transfer rate for a section of reactor between heights *j* and *k* is calculated as

$$v_{jk} = v_k - v_j \quad (9)$$

From equation (8), k_L values in two reactor sections, between *j* and *k*, and *h* and *i* heights respectively, can be related by the following equation:

$$k_{Ljk} = k_{Lhi} \cdot v_{jk} \cdot A_{hi} / v_{hi} \cdot A_{jk} \quad (10)$$

3.5. Residence time distribution

The residence time distribution (RTD) was experimentally studied at packed-bed heights of 0 to 84 cm. Air and liquid flow rates were 1.1L/min and 2.4 L/h respectively. Copper ion was used as a tracer. At a specific time (t = 0), 5 mL of a copper sulphate solution with 40 g/L of copper was injected quickly in one shot into the feed stream. The outlet copper concentration was then measured as a function of time.

3.6. Analytical methods

Ferrous iron concentration was determined by end-point automatic titration with 0.0083 M $K_2Cr_2O_7$. Copper concentration was determined by atomic absorption spectrophotometry. Titanium (III) concentration was analyzed by measuring the ferrous iron resulting from the reaction of Ti(III) with an excess of Fe(III) according to:

$Ti^{3+} + Fe^{3+} \rightarrow Ti^{4+} + Fe^{2+}$

(1 mL of problem solution plus 3 mL of ferric sulphate solution with 12 g/L of iron and pH=1.25; 1 minute of intensive mixing)

4. Results

4.1. Ferric iron productivity of the bioreactor

The bioreactor studied by Mazuelos et al. (2000) for the ferrous iron biooxidation was tested at various steady states. In the experimental conditions used, the biooxidation process was limited by the availability of oxygen in the liquid medium. The operating conditions and the ferric iron productivity obtained in each floor and the whole system were the following:

Steady state selected: air flow rate = 1095 mL/min

liquid flow rate = 2374 mL/h

Ferrous iron concentration in the inlet solution = 8.08 g/L (pH = 1.28)

Ferric iron productivity: zero floor = 1.14 g/h

first floor = 7.31 g/h

second floor = 4.89 g/h

third floor = 2.90 g/h

whole reactor = 16.24 g/h

4.2. Gas-liquid interfacial area

Fig. 2 shows the mean bubble diameter, d_b, and the volume occupied by gas, V_G, as a function of the packed-bed height. Table 1 shows the gas-liquid interfacial area calculated for different packed-bed sections.

4.3. Effect of the column height on the mass transfer coefficient value

Table 2 shows the gas-liquid oxygen transfer rate when $TiCl_3$ was present in the liquid medium, calculated from equation (8), at several packed bed heights. By applying equation (10), the following k_L relationships between different sections of the first floor and zero floor were obtained:

$$k_{L(0\text{-}10\ cm)} = 0.14 \cdot k_{L0} \quad (11)$$

$$k_{L(10\text{-}15\ cm)} = 0.50 \cdot k_{L0} \quad (12)$$

$$k_{L(15\text{-}20\ cm)} = 0.62 \cdot k_{L0} \quad (13)$$

$$k_{L(20\text{-}25\ cm)} = 0.59 \cdot k_{L0} \quad (14)$$

$$k_{L(25\text{-}28\ cm)} = 0.69 \cdot k_{L0} \quad (15)$$

4.4. Residence time distribution

Fig. 3 illustrates the normalized RTDs function, E(θ), at three packed-bed heights, calculated from pulse tracer experiments. The reactor has been modelled as equal size ideal continuous stirred tank reactors in series. The number of tanks in series necessary to model the reactor, N, is determined from the dimensionless variance, $\sigma\theta^2$, according to the following equation:

$$N = 1 / \sigma_\theta^2 = \tau^2 / \sigma^2 \quad (16)$$

where τ is the mean residence time and σ^2 is the variance calculated from the pulse tracer experiment. As the number of reactors increases, the behavior of the system approaches that of a plug-flow reactor

Table 3 shows the residence time distribution and model parameters at different packed-bed heights.

5. Discussion

Fig. 2 shows that the mean bubble size increased, as a result of a continuous coalescence process, as the height of the packed bed increases up to 20 cm. The mean bubble size remained almost constant at higher heights probably due to the fact that the bubble size became determined by the size of channels between the solid particles in the bed. It is the combination of smaller bubbles (larger specific interfacial area) with higher gas volume per unit of bed (slope of the V_G vs. height curve in Fig. 2) that promoted an enhanced oxygen transfer in the first floor since its gas-liquid interfacial area, calculated from Eq. (3), was higher than those of the second and third floors (Table 1). The same arguments are valid to explain the similar values of the gas-liquid interfacial area in second and third floors.

The stream of gas in the form of small bubbles leaving the diffuser was the main source of agitation in the reactor. Therefore, as a section of the reactor was closer to the air diffuser its degree of liquid axial mixing must be higher hence the liquid flow pattern approaches that of the ideal CSTR. Table 3 illustrates this effect in a quantitative

manner. In the first floor complete mixing as if in one well-mixed tank is found and for the whole column (84 cm) two well-mixed tanks simulate the flow pattern. Intensity of mixing therefore decreases with increasing distance above the inlet.

From Eqs. (11) to (15) it can be seen that the value of k_L in the zero floor, i. e. k_{L0}, was higher than those in any section of the first floor. This is due to the fact that, with regard to any section of bed, mixing was favoured in the zero floor by the presence of the air diffuser and the absence of support particles. Taking into account these arguments it can be postulated that the value of k_L in the zero floor (k_{L0}) was also higher than those in second and third floors.

The limitations of the methodology applied to the study of the oxygen transfer lie in the fact that an abiotic system is involved, which may differ from conditions present in a bioreactor with a biofilm on the support particles. Therefore, the application of absolute values of the parameters experimentally determined in this study to the bioreactor developed by Mazuelos et al. (2000) would be incorrect, mainly for the following reasons:

- In spite of the fact that both systems are geometrically similar and have the same type of solid particles forming the packed bed, passageways for gas and liquid in the bed will be different in size and shape (more or less tortuous) mainly due to the presence or absence of biofilm. This implies a liquid-bubble mixing pattern different in each system.
- In accordance with the methodology employed for the liquid flow model study, this is related to the bed height instead of to the vertical position in the whole reactor (including zero, 1st, 2nd and 3rd floors). In the whole reactor, at a certain vertical position "h" lower than its total height, the liquid flow is influenced by the motion of elements of fluid located both below "h" and above "h" .

- Owing to the presence of biomass in the bioreactor fluid characteristics (density, viscosity, surface tension, etc) might be different from those of the liquid used in this work. It is known that oxygen transfer is influenced by the presence of cells in fermentation broths (Doran, 1995). Cells interfere with bubble break-up and coalescence, and cells, proteins and other molecules which adsorbs at gas-liquid interfaces also cause interfacial blanketing which reduces the contact area between gas and liquid.

Taking into account the above mentioned statements it can be concluded that the relationships between the k_L values of different sections in the bioreactor would be different from those obtained in this work. However, it is possible to consider experimental results in a relative and qualitative way in order to describe the gas-liquid oxygen transfer in the bioreactor. It is postulated that the following results are valid in the bioreactor:

- The gas-liquid interfacial area of the first floor is higher than that of the second and third floors, these two being similar.
- The liquid axial mixing extent depends on the vertical location in the column, increasing as the proximity to the air diffuser increases.
- The k_L value in the zero floor, k_{L0}, (without bed) is higher than that in the 1^{st}, 2^{nd} and 3^{rd} floors (with packed bed).

By considering these results, an hypothesis is made to address how gas-liquid oxygen transfer contributes to explain the differences in the ferric iron productivity found in each floor of the bioreactor (Mazuelos 2000):

1) the oxygen transferred by bubbles housed in bed floors is almost totally consumed by the biomass living there, since the dissolved oxygen was the limiting agent of the biooxidation process in the steady state considered .

2) The oxygen transferred by bubbles housed in zero floor is no totally consumed by the biomass living there as there are good conditions for oxygen transfer (the highest gas-liquid interfacial area and the highest value of k_L in the column) and low biomass density because there is not inert support for biofilm formation.

3) The spare dissolved oxygen in zero floor is transported by the liquid moving upwards to other sections of the bioreactor where it is consumed by the biomass housed in the biofilm.

4) The amount of oxygen transported by the liquid moving upwards from zero floor to other sections of the bioreactor is proportional to the liquid axial mixing extent in them. Axial mixing allows in its turn that liquid moving downwards and passing through zero floor increases its dissolved oxygen concentration.

Now, ferric iron productivity differences can be understood. The highest ferric iron productity was obtained in the first floor due to its high gas-liquid interfacial area and to its high liquid axial mixing extent. The ferric iron productivity of the second floor was higher than that of third one due to the fact that, in spite of both floors having similar gas-liquid interfacial areas, the second floor has a liquid axial mixing extent higher than that of the third floor.

6. Conclusions.

In a packed-bed reactor for ferrous iron biooxidation the gas-liquid interfacial area per unit of bed height is not constant along the reactor, being higher in sections closer to the air diffuser. In spite of being a tubular reactor there are deviations from the plug-flow model that are higher as the reactor section is closer to the air diffuser. When

the dissolved oxygen is the limiting agent for the biooxidation process, the ferric iron productivity in a section of the reactor depends on the gas-liquid interfacial area and on the axial mixing extent of the section.

Acknowledgements.

The authors wish to acknowledge the financial support of CICYT (Cominsión Interministerial de Ciencia y Tecnología, Spain), Project BIO95 0482.

References.

Armentia H., Webb C., Ferrous sulphate oxidation using *Thiobacillus ferrooxidans* cells immobilized in polyurethane foam support particles, Appl. Microbiol. Biotechnol. 36, (1992), 697-700.

Carranza F., García M. J., Kinetic comparison of support materials in the bacterial ferrous iron biooxidation in packed-bed columns, Biorecovery 2, (1990), 15-27.

Carranza F., Iglesias N., Romero R., Palencia I., Kinetics improvement of high grade sulfides bioleaching by effect separation, FEMS Microbiol. Rev. 11 (1993) 129-138.

Doran P. M., 1995, Bioprocess engineering principles. Academic Press Ltd., 196-216.

García M.J., Palencia I., Carranza F., Biological ferrous iron in packed-bed columns with low-grades sulphide mineral as support, Process Biochem. 24, (1989), 84-87.

Gómez J. M., Cantero D., Soporte para la inmovilización de un catalizador, Ing. Quím. 354, (1999), 171-175.

Grishin S. I., Tuovinen O. H., Fast kinetics of Fe^{2+} oxidation in packed-bed reactors, Appl. Environ. Microbiol. 54 (12), (1988) 3092-3100.

Iglesias N., Palencia I., Carranza F., IBES process: description and applications, S. Afr. Inst. Min. Metall. (1996) 181-185, Hidden Wealth.

Karamanev D. G., Model of the biofilm structure of *Thiobacillus ferrooxidans*, J. Biotechnol. 20, (1991), 51-64.

Lancy E. D., Tuovinen O. H., Ferrous iron oxidation by *Thiobacillus ferrooxidans* immobilized in calcium alginate, Appl. Microbiol. Biotechnol. 20, (1984), 94-99.

Livesey-Goldblatt E., Tunley T. H., Nagy I. F., Pilot plant film oxidation (Bacfox process) of recycled acidified Uranium plant sulphate leach solution, in: Schwartz (Ed.), Conference Bacterial Leaching, Verlag Chemie, Wein-heim, FRG, (1979), 175-190.

Magota H., Shiratori Y., Treatment of sour natural gas containing hydrogen sulfide, Jpn. Kokai Tokkyo Koho, Japanese patent no. 63 205 124, (1988).

Mazuelos A., Romero R., Palencia I., Iglesias N., Carranza F., Continuous ferrous iron biooxidation in flooded packed-bed reactors, Miner. Eng. 12, (1999), 559-564.

Mazuelos A., Carranza F., Palencia I., Romero R., High efficiency reactor for the biooxidation of ferrous iron, Hydrometallurgy 58 (2000) 269-275.

Mazuelos A., Palencia I., Romero R., Rodríguez G., Carranza F., Ferric iron production in packed bed bioreactors: influence of pH, temperature, particle size, bacterial support material and type of air distributor, Miner. Eng. 5 (14), (2001), 507-514.

Nakamura T., Nokie K., Matsumoto J., Effect of operational conditions on biological Fe(II) oxidation with rotating biological contactors. Water Res. 20, (1986), 73-77.

Nikolov L., Valkova-Valchanova M., Mehochev D., Oxidation of high ferrous iron concentrations by chemolithotrophic *Thiobacillus ferrooxidans* in packed-bed bioreactors, J. of Biotechnol. 7, (1988), 87-94.

Oliveira M. S. N., Ni X., Gas hold-up and bubble diameters in a gassed oscillatory baffled column, Chem. Eng. Sci. 56, (2001), 6143-6148

Table captions:

Table 1

Gas-liquid interfacial area in different sections of the reactor

Table 2

Gas-liquid oxygen transfer when $TiCl_3$ was present in the liquid medium

Table 3

Parameters used to characterize RTD

Figure captions:

Figure 1

Simplified flowsheets of the indirect bioleaching with effects separation process and the desulfuration of gaseous fuels.

Figure 2

Effect of the packed-bed height on the mean bubble size and the gas volume

Figure 3

RTD curves for different bed heights. Air flow rate: 1.1 L/min, liquid flow rate: 2.4 L/h

Tables:

Table 1

Packed bed zone	Gas-liquid Interfacial area a_{jk} (cm^2)	Gas-liquid Interfacial area (cm^2)
Zero floor	8265	Zero floor: 8265
0-2 cm	3203	First floor: 7008
2-4 cm	818	
4-6 cm	589	
6-8 cm	362	
8-10 cm	239	
10-12 cm	247	
12-15 cm	175	
15-20 cm	497	
20-25 cm	402	
25-28 cm	476	
28-56 cm	3861	Second floor: 3861
56-84 cm	4183	Third floor: 4183

Table 2

Packed bed heights (cm)	gas-liquid transfer rate (vj)(moles O_2/s)	gas-liquid transfer rate (moles O_2/s)
0	$3.11 \cdot 10^{-6}$	Zero floor (v_0): $3.11 \cdot 10^{-6}$
10	$3.39 \cdot 10^{-6}$	First floor (v_{28}-v_0): $6.90 \cdot 10^{-7}$
15	$3.47 \cdot 10^{-6}$	
20	$3.59 \cdot 10^{-6}$	
25	$3.68 \cdot 10^{-6}$	
28	$3.80 \cdot 10^{-6}$	

Table 3

Packed-bed heights (cm)	τ (min)	σ^2 (min^2)	σ_θ^2	N
Zero floor	22.68	446.08	0.87	1.15
2	21.58	417.90	0.90	1.11
4	22.11	394.94	0.81	1.24
6	22.43	403.36	0.80	1.25
8	23.82	454.47	0.80	1.25
10	24.19	449.09	0.77	1.30
12	24.82	455.19	0.74	1.35
15	25.93	474.43	0.71	1.42
20	27.79	535.97	0.69	1.44
25	29.32	556.64	0.65	1.54
28	30.70	595.82	0.63	1.59
84	67.78	1964.3	0.43	2.34

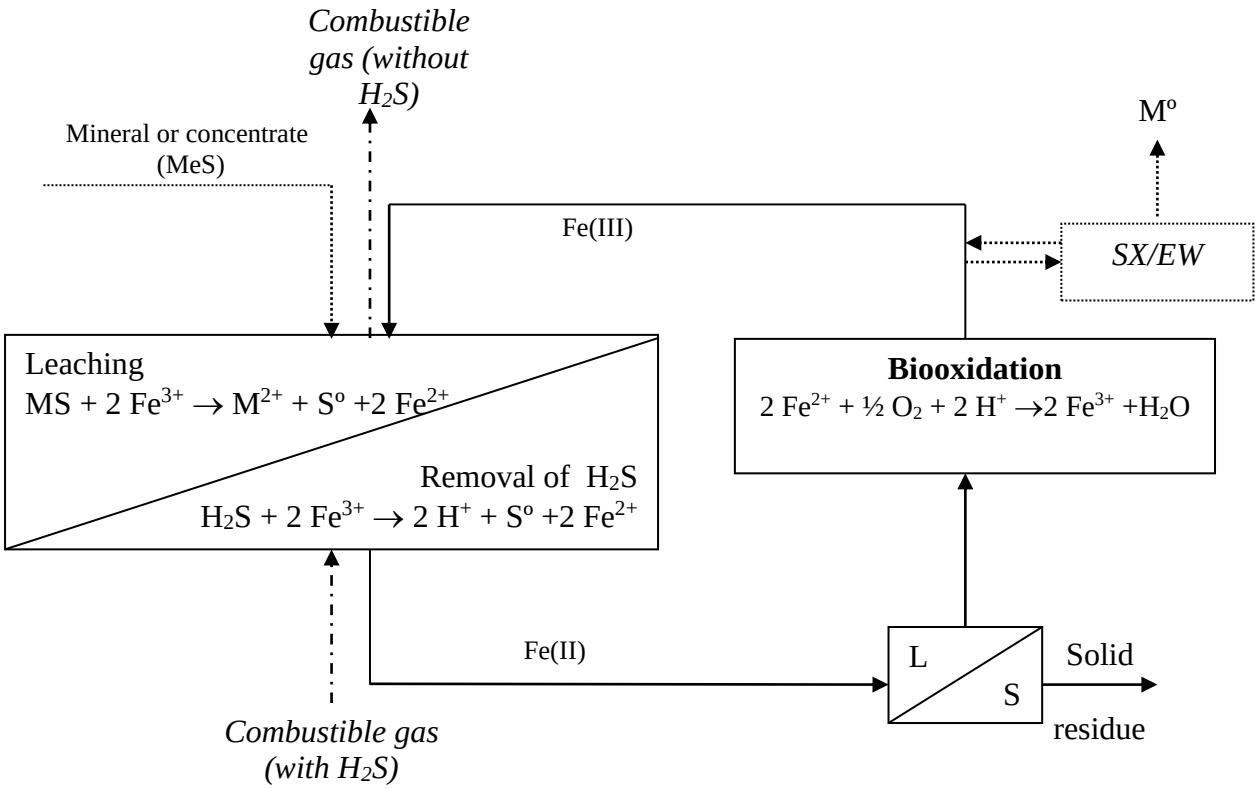
Combustible gas (without H_2S)
Mineral or concentrate (MeS)
Mº
Fe(III)
SX/EW
Leaching
MS + 2 Fe^{3+} → M^{2+} + Sº +2 Fe^{2+}
Removal of H_2S
H_2S + 2 Fe^{3+} → 2 H^+ + Sº +2 Fe^{2+}
Biooxidation
2 Fe^{2+} + ½ O_2 + 2 H^+ →2 Fe^{3+} +H_2O
Fe(II)
L
S
Solid
residue
Combustible gas (with H_2S)

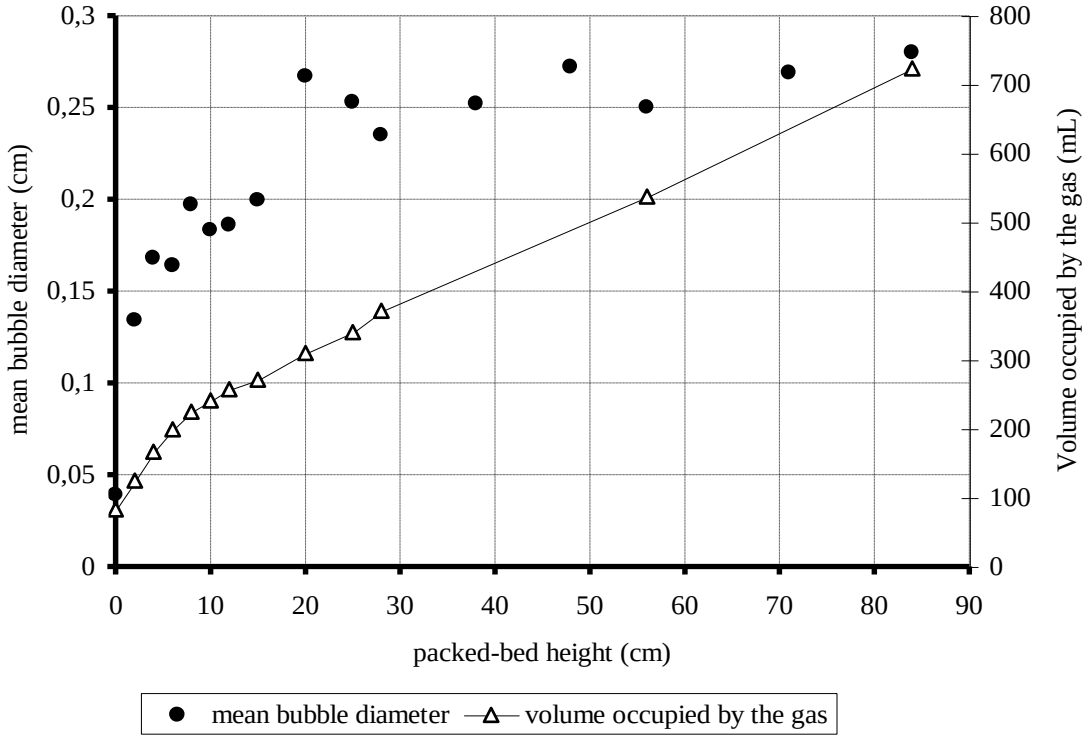
0,3
0,25
0,2
0,15
0,1
0,05
0
mean bubble diameter (cm)
800
700
600
500
400
300
200
100
0
Volume occupied by the gas (mL)
0
10
20
30
40
50
60
70
80
90
packed-bed height (cm)
mean bubble diameter
volume occupied by the gas

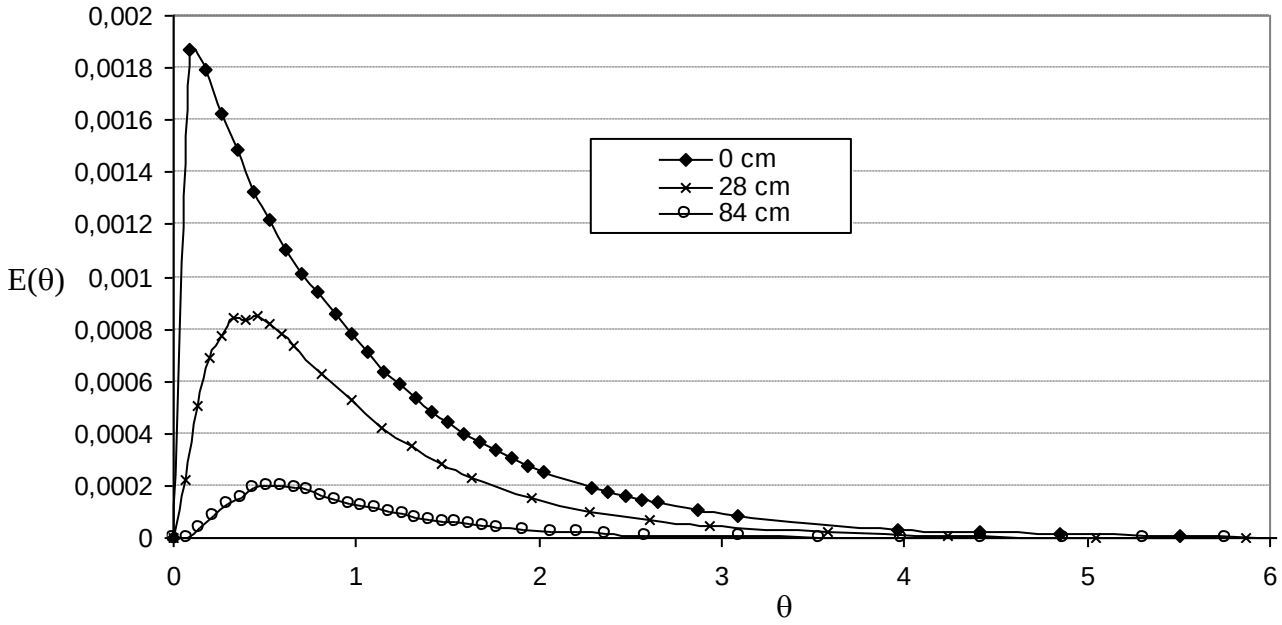
0,002
0,0018
0,0016
0,0014
0,0012
0,001
0,0008
0,0006
0,0004
0,0002
0
E(θ)
0 cm
28 cm
84 cm
0
1
2
3
4
5
6
θ